Mass-producible near-body temperature-triggered 4D printed shape memory biocomposites and their application in biomimetic intestinal stents

Cheng Lin [a], Zhipeng Huang [c], Qinglong Wang [c], Zhichen Zou [d], Wenbo Wang [d], Liwu Liu [b,**], Yanju Liu [b], Jinsong Leng [a,*]

[a] Centre for Composite Materials and Structures, Harbin Institute of Technology, No. 2 Yikuang Street, Harbin, 150001, PR China
[b] Department of Astronautical Science and Mechanics, Harbin Institute of Technology, No. 92 West Dazhi Street, Harbin, 150001, PR China
[c] Tangdu Hospital of the Air Force Military Medical University, No. 1, Xinsi Road, Xi`an, 710038, PR China
[d] The First Affiliated Hospital of Harbin Medical University, No. 23 Youzheng Street, Nangang District, Harbin, 150001, PR China

ARTICLE INFO

ABSTRACT

Despite the burgeoning interest in manufacturing highly complex and dynamically reconfigurable implants using the 4D printing technique, one of the most critical challenges is to develop near-body temperature (NBT)-triggered 4D printing materials in a facile and scale-up manner. The currently reported 4D printed biomaterials for implants have inappropriate transition temperatures or are limited to demonstration production of small amounts of materials in the laboratory. Here, 4D printed shape memory biocomposites with controllable transition temperature were developed through facile manufacturing technology, and the shape memory process of triggering printed constructs under NBT was realized. Customized, reconfigurable, biodegradable, and biocompatible 4D printed biomimetic intestinal stents were developed using NBT-triggered biocomposites, filling the blank of 4D printed intestinal stents. The 4D printed biomimetic intestinal stents were designed based on wavy biomimetic networks that can mimic the nonlinear stress-strain response of biological tissues, demonstrating high flexibility and facilitating reduced irritation of the intestinal wall. More importantly, the biodegradability of the 4D printed biomimetic intestinal stent can avoid the secondary endoscope removal required by the metal intestinal stent. This work not only offers an efficient and facile methodology to fabricate NBT-triggered 4D printing shape memory biocomposites but also demonstrates the attractive application potential of 4D printed intestinal stents in next-generation intelligent implants.

1. Introduction

Traditional implantable medical devices usually have only a few specific geometric specifications. However, the geometric configuration mismatch between implantable devices and lesions often leads to an increased risk of complications and even failure of surgery [1–4]. These limitations have spurred the development of personalized medicine, which is tailor-made treatments for individuals rather than a broad group of patients. 3D printing is a technology that is closely linked to personalized medicine by designing sophisticated implants with patient-oriented dimensions and configurations [5,6]. The 4D printing strategy is based on integrating active biomaterials (e.g., bio-based shape memory polymers (SMP)) into 3D printing, with the embedding capability of time-varying shape reconfiguration in response to external

stimuli [7–15]. This advanced strategy not only enables complex personalized implants but also offers great potential for creating dynamic structures to achieve exciting functions, such as imitating the dynamic growth mechanisms of biological tissues/organs, reducing invasive damage to tissues during implantation, etc. [11,16–18]. Morrison et al. developed polycaprolactone (PCL)-based 4D printed personalized stents to treat patients with tracheobronchomalacia. Long-term data showed that the stent could adapt to tissue growth over time, which could avoid the migration problems and frequent size adjustments caused by the current fixed model and size of stents [19].

Many soft biological tissues, such as cardiac muscles, blood vessels, and intestines, exhibit nonlinear J-shaped stress-strain response ("strain stiffing"), which is a contribution of the wavy elastin and collagen fibers in the tissue [17,20,21]. During the loading process, the curved fibers
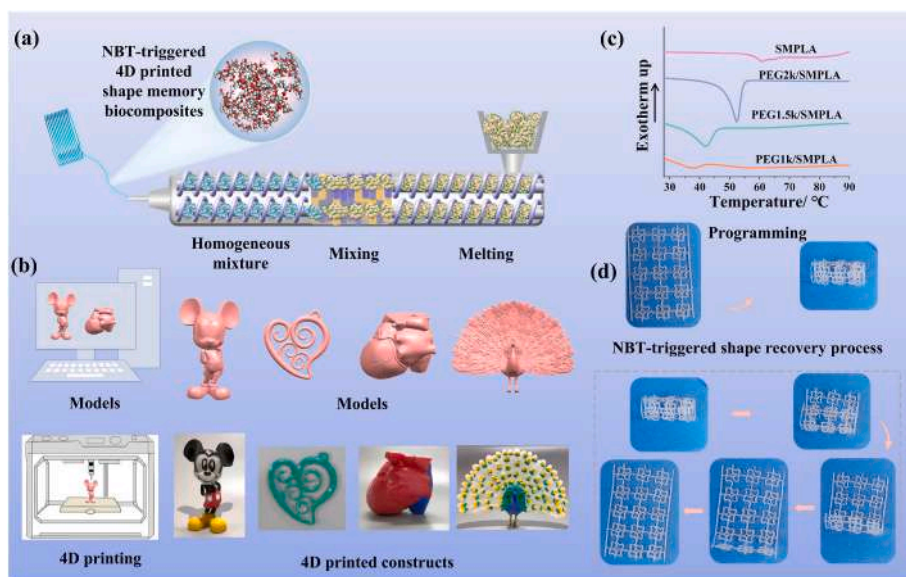

Fig. 1. (a) Preparation of NBT-triggered 4D printed shape memory biocomposites. (b) Digital models and 4D printed constructs. The printed constructs were colored for clarity of demonstration. (c) DSC curves of SMPLA and PEG/SMPLAs. (d) The NBT-triggered shape recovery process of the 4D printed shape memory PEG/SMPLA architecture.

first undergo untwisting, which manifests as a low modulus under small strains. As the strain increases, the curved microstructures of fibers are stretched into straight microstructures, resulting in a dramatic increase of modulus after experiencing a transition region. Inspired by the collagen fibers, a variety of wavy biomimetic metamaterial networks have been designed to mimic the J-shaped mechanical behavior of biological tissues, demonstrating the exclusive advantages of adaptability to biological tissues and structural flexibility [20,21]. Ma et al. developed biomimetic networks with horseshoe shaped microstructures, and established theoretical models between the geometric parameters and mechanical behavior of networks. Based on the theoretical model, the J-shaped stress-strain behavior of skin was reproduced [21]. In addition, many other biomimetic metamaterials have been developed, such as metamaterials with a wide range of CTE values, metamaterials with controlled thermomechanical stability, and metamaterials with tunable thermal expansion properties [22–30]. However, the application of wavy biomimetic metamaterial networks in implantable devices has rarely been explored. Notably, the implantable devices based on wavy biomimetic networks can realize the co-deformation of the device and biological tissue under small strains, which can prevent tissue wear and even perforation caused by the large difference in mechanical properties between the tissue and the device. Under large strains, the "strain stiffness" response of the biomimetic network enables the device to avoid mechanical failures caused by excessive deformation.

Although 4D printing has shown great advantages in preparing intelligent implants, such as customizability, self-adaptability, and minimal invasiveness [17,18], one of the most critical challenges is to develop near-body temperature (NBT)-triggered 4D printed biomaterials in a facile and accessible way. Shape memory biomaterials such as shape memory polylactic acid (SMPLA) and shape memory polycaprolactone (SMPCL) have undesirable shape memory temperatures, which may adversely affect tissues during implant deployment [31,32]. Or, even if the transition temperature is tunable, the material preparation process is extremely cumbersome. As a result, the material can only be limited to demonstration applications at the laboratory stage and cannot be scaled up to provide a possibility for the widespread clinical use of 4D printed implants.

Here, NBT-triggered 4D printed shape memory biocomposites based on polyethylene glycol (PEG)/SMPLA were developed through melt extrusion, with the advantages of simplicity, scalable production,

biodegradability, biocompatibility, and reconfigurability. 4D printed constructs were fabricated by fused deposition modeling (FDM) printing method because FDM does not involve organic solvents or toxic photoresins, thus potential health risks or other barriers to clinical application are avoided. The biodegradation behavior was studied to examine the evolution of the mechanical properties and weight loss of the biocomposites. The association between toughness and fracture morphology of mechanical test specimens was explored. The cytocompatibility and histocompatibility of 4D printed biocomposites were verified by co-culture with intestinal cells and in vivo implantation in mice. Additionally, biomimetic networks with different wavy structures were designed and fabricated using the NBT-triggered 4D printed shape memory biocomposites, which showed the J-shaped mechanical properties similar to biological tissues. Biomimetic intestinal stents were designed based on biomimetic networks, which realized reconfigurable shape recovery and reopen the simulated narrow intestine, proving the effectiveness and functionality of the intestinal stent.

2. Results and discussion

The schematic of the 4D printed shape memory PEG/SMPLA biocomposite filaments prepared by melt extrusion is shown in Fig. 1a. The 4D printed PEG/SMPLA biocomposite filaments were capable of printing complex structures such as mice, pendants, hearts, and peacocks with high quality using a commercial FDM 3D printer (Fig. 1b, Fig. S1), demonstrating the excellent printing performance. To obtain the transition temperatures of 4D printed shape memory PEG/SMPLA biocomposites, the thermal behavior was analyzed by differential scanning calorimetry (DSC, Fig. 1c). For SMPLA and its composites, the glass transition temperature (T_g) is the shape transition temperature. The results showed that the T_g of PEG/SMPLA was significantly lower than that of pure SMPLA, which was because the plasticizing effect of low molecular weight PEG reduced the interaction between SMPLA molecular chains. The plasticizing effect became more pronounced as the molecular weight of PEG decreased. The T_g of PEG1k/SMPLA, PEG1.5k/SMPLA, and PEG2k/SMPLA were approximately 38 °C, 42 °C, and 52 °C, respectively. The continuous and controllable adjustment of T_g of 4D printed biocomposites can be realized by adjusting the molecular weight and content of PEG, and the ideal transition temperature can be obtained. To evaluate the reconfigurable shape memory performance of 4D
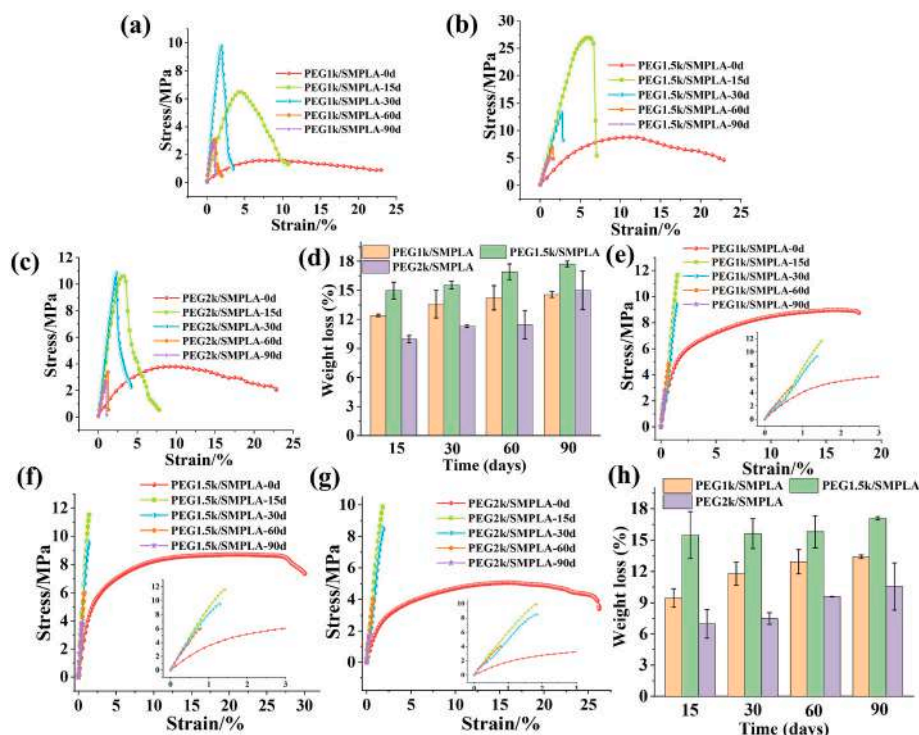
Fig. 2. (a–c) Flexural tests of PEG/SMPLAs. Stress-strain curves of (a) PEG1k/SMPLA, (b) PEG1.5k/SMPLA, and (c) PEG2k/SMPLA under flexural loading after different biodegradation times. (d) Weight loss of flexural specimens. (e–g) Tensile tests of PEG/SMPLAs. Stress-strain curves of (e) PEG1k/SMPLA, (f) PEG1.5k/SMPLA, and (g) PEG2k/SMPLA under tensile loading after different biodegradation times. (h) Weight loss of tensile specimens.

printed shape memory biocomposites, a planar network architecture was prepared by PEG1.5k/SMPLA filaments and then shaped into a coiled temporary configuration. The architecture in the temporary configuration enabled dynamic shape recovery to its initial configuration at NBT (42.5 °C–43.1 °C), demonstrating excellent shape memory performance. The reconfigurable shape recovery process with real-time temperature monitoring is shown in Fig. S2.

For 4D printed shape memory implants, ideally, the shape memory temperature should be slightly higher than the body temperature (e.g., 42 °C–43 °C), in which case the implant will show exclusive advantages. This is because the tissue will not be damaged by excessively high or low temperatures, and the implant in the rubber state during the implantation process can greatly reduce the tissue infiltration damage caused by the implantation. In addition, after implantation, the 4D printed shape memory implant is in a glassy state at body temperature, which can provide sufficient mechanical support for the lesion, thereby avoiding the risk of collapse that may be caused by conventional polymers. Hence, PEG1.5k/SMPLA was selected as the preferred NBT-triggered 4D printed shape memory biocomposite.

The prepared shape memory PEG/SMPLA biocomposites will be used as raw materials for 4D printed implants. Therefore, it is necessary to evaluate the mechanical properties of PEG/SMPLA biocomposites and the effect of biodegradation on their mechanical properties, as the implants will be in a physiological environment. First, the flexural performance and the evolution of flexural performance with biodegradation time were examined (Fig. 2a–c, Fig. S3). Without biodegradation (0 d), PEG1k/SMPLA, PEG1.5k/SMPLA, and PEG2k/SMPLA showed no fracture phenomenon within the loading range due to their high toughness. With the increase of biodegradation time, the stability of the molecular chain decreased gradually because of hydrolysis, leading to the decrease of flexural strength and elongation at break of PEG/SMPLAs. After 15 days of biodegradation, although the toughness of the PEG/SMPLAs decreased, the elongation at break of PEG1k/SMPLA, PEG1.5k/SMPLA, and PEG2k/SMPLA remained at

approximately 11%, 7%, and 7%. PEG1.5k/PLA showed higher flexural strength than PEG1k/SMPLA and PEG2k/SMPLA, probably due to its superior melting extrusion processability and printability. After 30 days of biodegradation, the flexural strengths of PEG1k/SMPLA, PEG1.5k/SMPLA, and PEG2k/SMPLA were about 10 MPa, 13 MPa, and 11 MPa, respectively. Besides, the weight loss rate of PEG/SMPLAs increased with biodegradation time because of the detachment of biodegradation products (e.g., oligomers and monomers) from the matrix (Fig. 2d), demonstrating the biodegradability of PEG/SMPLAs. After 90 days of biodegradation, the weight loss rates of PEG1k/SMPLA, PEG1.5k/PLA, and PEG2k/SMPLA flexural specimens were 14.6%, 17.7%, and 15.0%, respectively.

In addition, the tensile performance of the 4D printed shape memory PEG/SMPLA biocomposites was investigated (Fig. 2e–g, Fig. S4). Similarly, without biodegradation (0 d), PEG1k/SMPLA, PEG1.5k/SMPLA, and PEG2k/SMPLA exhibited excellent toughness. The long fiber protrusions in the longitudinal fracture morphology were associated with the high elongation at break of PEG/SMPLAs, as the fiber protrusions can absorb more energy (Fig. S5a). On the 15th day of biodegradation, the tensile strengths of PEG1k/SMPLA, PEG1.5k/SMPLA, and PEG2k/SMPLA were 11.7 MPa, 11.6 MPa, and 10.0 MPa, respectively. The elongation at break decreased with the biodegradation time, and correspondingly, the morphology became smoother with fewer features (Figs. S5b and c). The cross-sectional morphology showed a similar trend (Fig. S6), changing from independent fibrous protrusions (undegraded) to a monolithic block (degraded for 90 days). After 90 days of biodegradation, the weight loss rates of PEG1k/SMPLA, PEG1.5k/SMPLA, and PEG2k/SMPLA tensile specimens were 13.4%, 17.1%, and 10.6%, respectively (Fig. 2h). The slight difference in weight loss rate between rectangular flexural specimens and dog-bone tensile specimens indicated that the biodegradation rate was affected not only by the material composition of the specimens but also by the geometry of the specimens.

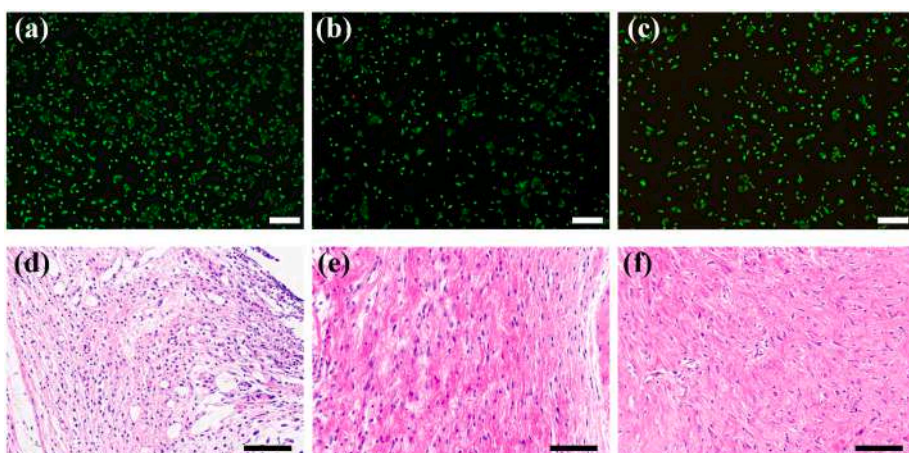To assess the cytocompatibility of 4D printed shape memory PEG/

Fig. 3. Merged fluorescent images of cells co-cultured with 4D printed shape memory (a) PEG1k/SMPLA, (b) PEG1.5k/SMPLA, (c) PEG2k/SMPLA biocomposites. The living cells were stained green, and the dead cells were stained red. Scale bar: 250 μm. Histological examination of 4D printed shape memory PEG1.5/SMPLA biocomposites implanted subcutaneously in mice. Implanted for (d) 7 days, (e) 30 days and (f) 60 days. Scale bar: 100 μm. (For interpretation of the references to color in this figure legend, the reader is referred to the Web version of this article.)
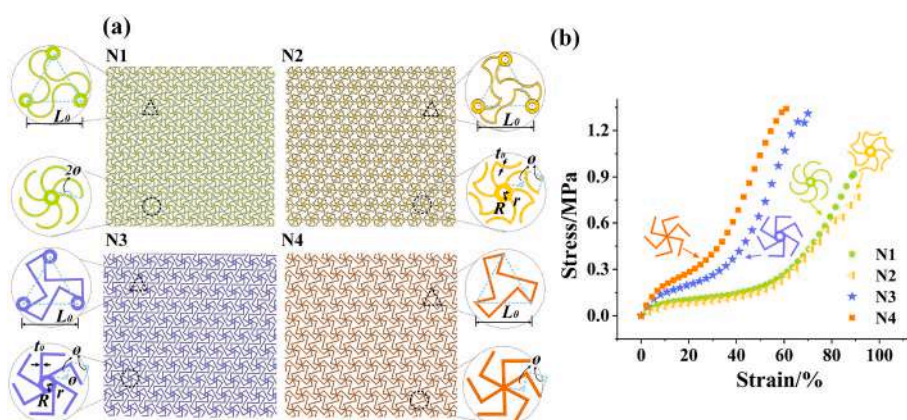

Fig. 4. (a) Structures and geometric parameters of the designed biomimetic networks. (b) Tensile tests of biomimetic networks.

SMPLA biocomposites, co-culture of PEG/SMPLAs with intestinal cells was performed. Fig. 3a–c shows merged fluorescence images of intestinal cells, in which the living cells are displayed in green and the dead cells are displayed in red. It can be seen that the three PEG/SMPLAs showed no negative effects on the survival state of cells, and the cells maintained high viability, indicating their good cytocompatibility. Besides, the in vivo histocompatibility of the 4D printed shape memory PEG/SMPLA biocomposites was characterized by subcutaneous
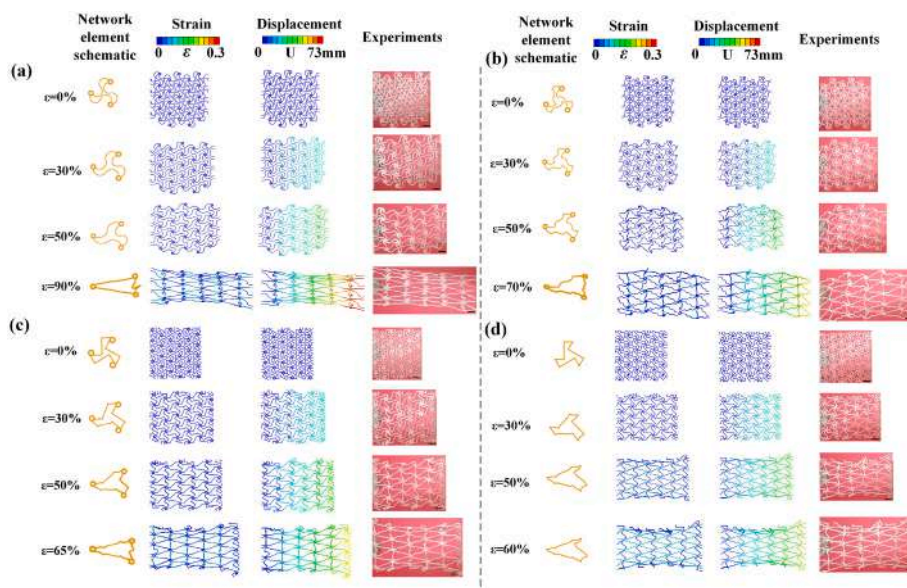

Fig. 5. Experimental and simulation analysis of biomimetic networks under different levels of tensile loading. (a) N1, (b) N2, (c) N3, and (d) N4 biomimetic networks. Scale bar: 10 mm.

implantation in mice. Histological analysis revealed a significant inflammatory cell infiltration 7 days after implantation (Fig. 3d), which was due to the self-protective mechanism of the foreign body reaction initiated by the host mice. The PEG/SMPLAs were encapsulated by a non-specific protein layer after implantation, and inflammatory cells were exuded from the vessels. At 30 days, the inflammation response gradually subsided (Fig. 3e). At 60 days, inflammatory cells continued to decrease, revealing dense connective tissue and well-arranged fibrous tissue (Fig. 3f). The three PEG/SMPLAs exhibited similar reaction phenomena, which indicated that foreign PEG/SMPLAs were all accepted by the host and showed satisfactory histocompatibility in vivo.

The wavy biomimetic networks are able to exhibit stress-strain behaviors similar to biological tissues, thus greatly reducing the risk of tissue wear and even perforation [17,33–35]. Due to this unique advantage, four wavy biomimetic networks were developed and employed as the basis for the structural design of intestinal stents. Fig. 4a shows the models of the designed biomimetic networks. The representative unit of the N1 biomimetic network consists of a circular central node and six semicircular ligaments with a radian of 2Ø; the representative unit of the N2 biomimetic network is composed of a circular central node and six ligaments connected by two arcs with a radian of Ø; the representative unit of the N3 biomimetic network consists of a circular central node and six right-angle ligaments; the representative unit of the N4 biomimetic network is directly composed of six right-angled ligaments without a circular central node. The dimensionless design geometric parameters of the representative unit of the biomimetic network are $\emptyset = \pi/2$, $R/L_0 = 0.13$, $r/R = 0.5$, $t_0/L_0 = 0.04$. The mechanical properties of four biomimetic networks were characterized (Fig. 4b), and the four networks exhibited J-shaped stress-strain behavior similar to that of biological tissues [17,33–35]. The J-shaped stress-strain curve was divided into three phases. The first phase was the low modulus phase, the modulus rose slowly in the second phase, and the modulus rose rapidly in the third phase. The structural equivalent stiffness of the right-angled ligament networks (N3 and N4) was higher than that of the arc-shaped ligament networks (N1 and N2), while the arc-shaped ligament networks were more ductile, with elongation at break up to ~90% for both N1 and N2 biomimetic networks.

The deformation behaviors of the biomimetic networks under different levels of tensile loading were analyzed, and the deformation sequences obtained by experiments and simulations were in good agreement (Fig. 5). The analysis of the strain distributions of biomimetic networks showed that the strains of the ligament segments closely connected to the nodes were higher, while the strains of the ligament segments slightly distant from the nodes were lower. The deformation process of biomimetic networks was shown in the following three phases: In the initial phase of loading, the ligament deformation was dominated by bending, which corresponded to the low modulus stage in the J-shaped stress-strain curve in Fig. 4b. Then, the ligament was gradually straightened and the node began to rotate due to the deformation of the ligament. The ligament deformation entered the transition phase from "bending dominant" to "stretching dominant", corresponding to the phase of slowly rising modulus. Finally, the ligament was almost straightened. The deformation was completely dominated by stretching, and the modulus increased sharply. The schematics of network elements at different strains more clearly demonstrated the deformation of the ligaments and nodes during loading.

3. Application

Intestinal obstruction is a common complication of intestinal diseases and will be life-threatening if timely decompression is not performed. Although metal intestinal stents have been widely used to expand the obstructed intestinal lumen, they may cause problems such as mucosal hyperplasia, abrasion, perforation, and re-obstruction. In particular, when used for benign intestinal obstruction (e.g., Crohn's disease, ischemic enteritis), metal stents require secondary endoscopic
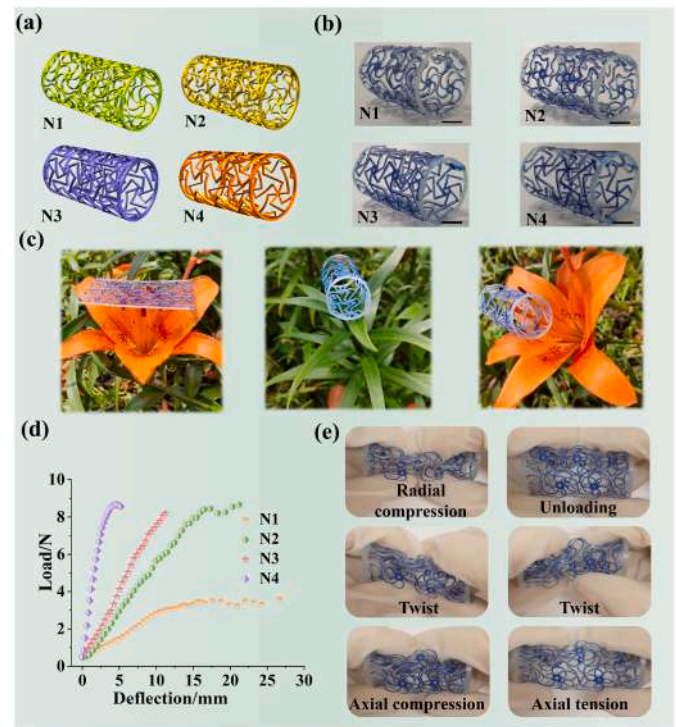

Fig. 6. (a) 3D models and (b) photographs of the 4D printed shape memory biomimetic intestinal stents. Scale bar: 10 mm. (c) Lightweight demonstration of the biomimetic networks and intestinal stents. (d) Compression behaviors of the 4D printed shape memory biomimetic intestinal stents. (e) Flexibility demonstration of the N1 4D printed shape memory biomimetic intestinal stent. The biomimetic stent can automatically return to its original configuration after being subjected to loads in different directions such as radial compression, axial tension, or torsion. The networks and stents were colored blue for clear display. (For interpretation of the references to color in this figure legend, the reader is referred to the Web version of this article.)

removal, which not only greatly increases the risk of complications, but also increases the pain and economic burden of patients [36–38]. To address the problems of metal stents, biodegradable polymeric intestinal stents were developed. For example, biodegradable polydioxanone (PDO) colorectal stents loaded with 5-fluorouracil (5-FU) were developed [37]. In addition, PDO biodegradable colorectal stents loaded with curcumin (CUR) and 5-FU were developed to induce tumor cell apoptosis [38] However, these biodegradable intestinal stents still suffer from complications due to size mismatch. Here, 4D printed shape memory biomimetic intestinal stents were developed, with prominent advantages of customization, self-adaptability, biodegradability, and biocompatibility. Due to the unique wavy biomimetic networks, the 4D printed shape memory intestinal stents exhibited significantly improved flexibility, which facilitated stents to conform to the peristaltic deformation of the intestine, thus reducing damage to the intestinal wall. Besides, the dynamically reconfigurable shape memory performance and the feasibility of reopening the obstructed intestine were examined.

The 4D printed shape memory intestinal stents with the wavy biomimetic structure were obtained by extending the 2D wavy biomimetic networks to 3D networks (Fig. 6a). Biomimetic intestinal stents were prepared by 4D printing using NBT-triggered shape memory PEG1.5k/SMPLA to achieve biodegradability, biocompatibility and configuration customization of stents (Fig. 6b). Furthermore, the advantages of 4D printed shape memory implants can be maximized under NBT triggering (transition temperature ~42 °C). For example, the impact of inappropriate transition temperature on the tissue can be avoided; the flexibility of the temporary configuration of the implant facilitates minimally invasive procedures; the implant is able to provide satisfactory support
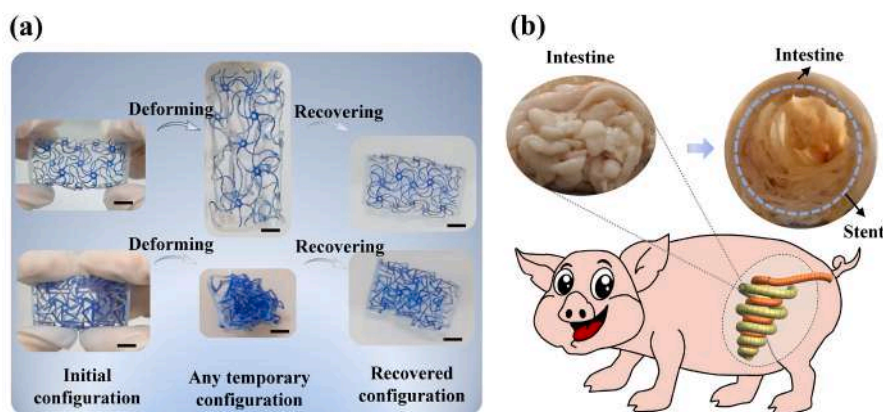
Fig. 7. (a) Dynamically reconfigurable shape memory performance of 4D printed biomimetic stents. The biomimetic stents were colored blue for clear display. Scale bar: 10 mm. (b) Feasibility of the 4D printed shape memory biomimetic stent opening simulated obstructed swine intestine. (For interpretation of the references to color in this figure legend, the reader is referred to the Web version of this article.)

for the lesion because it is glassy at body temperature. The lightweight biomimetic networks and stents can be stably placed on flowers or leaves (Fig. 6c), and thus will not cause excessive pressure on the intestine. In addition, the compression behaviors of the 4D printed shape memory biomimetic intestinal stents were examined (Fig. 6d). The N4 biomimetic stent possessed the largest structural equivalent stiffness, followed by the N3 and N2 biomimetic stents. The N1 biomimetic stent possessed the lowest structural equivalent stiffness but the best structural flexibility. The maximum compression loads that N2, N3, and N4 biomimetic stents can bear were similar, slightly higher than 8 N. Although the maximum compression load that the N1 biomimetic stent can withstand was slightly lower, its deformation ability was significantly better than the other three stents. During compression loading, the maximum deflection of the N1 biomimetic stent was 2.4 times that of the N3 biomimetic stent and 5.1 times that of the N4 biomimetic stent. The high structural flexibility of the N1 stent was further validated by applying loads in various directions. The N1 biomimetic stent can automatically return to its original structure after bearing loads in various directions and undergoing large deformation, which further validated its high structural flexibility (Video S1, Fig. 6e). The high flexibility of the N1 biomimetic stent was conducive to the coordinated deformation of the stent with the intestine, thus reducing the irritation to the intestinal wall.

Supplementary data related to this article can be found at https://doi.org/10.1016/j.compositesb.2023.110623.

Then, the dynamic reconfigurability of the 4D printed shape memory biomimetic stents was evaluated. The biomimetic stents exhibited outstanding programming flexibility and can be programmed to desired temporary configurations, such as auxetic temporary configuration and small-volume temporary configuration (Fig. 7a). The small-volume temporary configuration of the biomimetic stent was conducive to minimally invasive implantation. Then, biomimetic stents were capable of recovering to their original configurations under thermal stimulation, demonstrating excellent shape memory performance. More importantly, even after five shape memory cycles, the 4D printed biomimetic stent can still be fixed to the temporary configuration and return to the original configuration, which further proved the distinguished programmability and reconfigurability (Video S2). Besides, the 4D printed biomimetic stent was able to open the simulated obstructed swine intestine and restore the size of the intestinal lumen, which preliminarily proved the feasibility of the biomimetic stents for intestinal obstruction (Fig. 7b).

Supplementary data related to this article can be found at https://doi.org/10.1016/j.compositesb.2023.110623.

4. Conclusions

In summary, mass-producible NBT-triggered 4D printed shape memory biocomposites were developed with biodegradable, biocompatible, and dynamically reconfigurable properties. The 4D printed intestinal stents were developed for the first time and had the advantages of high flexibility, biodegradability, biocompatibility, and configuration customization, which can avoid secondary surgery and reduce the risk of complications. The printed constructs allowed the dynamically reconfigurable shape memory process to be completed at NBT (42 °C–43 °C), maximizing the advantages of 4D printed shape memory implants. The 4D printed biomimetic intestinal stents exhibited high reconfigurability and the ability to reopen the obstructed colon. This work provides a facile strategy to create attractive intelligent medical implants for tissue engineering in a rapid, precise, and customized manner. Of importance here is that the entire process, including preparing NBT-triggered 4D printed shape memory biocomposites, printing intestinal stents, and shaping temporary configurations of stents, does not involve any toxic solvents and can be readily scalable, further illustrating the high feasibility of this strategy for clinical application.

Author statement

Cheng Lin: Conceptualization, Investigation, Visualization, Writing-original draft. Zhipeng Huang: Investigation, Validation. Qinglong Wang: Investigation, Validation. Liwu Liu: Investigation, Resource, Supervision, Validation. Yanju Liu: Supervision, Visualization, Writing-review & editing. Jinsong Leng: Supervision, Visualization, Writing-review & editing.

Declaration of competing interest

The authors declare that they have no known competing financial interests or personal relationships that could have appeared to influence the work reported in this paper.

Data availability

Data will be made available on request.

Appendix A. Supplementary data

Supplementary data to this article can be found online at https://doi. org/10.1016/j.compositesb.2023.110623.

References

[1] Masura J, Gavora P, Formanek A, Hijazi ZM. Transcatheter closure of secundum atrial septal defects using the new self-centering amplatzer septal occluder: initial human experience. Cathet Cardiovasc Diagn 1997;42(4):388–93.
[2] Chessa M, Carminati M, Butera G, Bini RM, Drago M, Rosti L, et al. Early and late complications associated with transcatheter occlusion of secundum atrial septal defect. J Am Coll Cardiol 2002;39(6):1061–5.
[3] Lysitsas DN, Wrigley B, Banerjee P, Glennon PE, Parmar JM, Shiu MF, et al. Presentation of an embolised Amplatzer septal occluder to the main pulmonary artery 2 years after implantation. Int J Cardiol 2009;131(3):e106–7.
[4] Amin Z, Hijazi ZM, Bass JL, Cheatham JP, Hellenbrand WE, Kleinman CS. Erosion of Amplatzer septal occluder device after closure of secundum atrial septal defects: review of registry of complications and recommendations to minimize future risk. Cathet Cardiovasc Interv 2004;63(4):496–502.
[5] Prendergast ME, Burdick JA. Recent advances in enabling technologies in 3D printing for precision medicine. Adv Mater 2020;32(13):1902516.
[6] Lin C, Huang Z, Wang Q, Wang W, Wang Z, et al. 3D printed bioinspired stents with photothermal effects for malignant colorectal obstruction. Research 2022;2022:1–12.
[7] Xia Y, He Y, Zhang F, Liu Y, Leng J. A review of shape memory polymers and composites: mechanisms, materials, and applications. Adv Mater 2020:2000713.
[8] Xin X, Liu L, Liu Y, Leng J. 4D printing auxetic metamaterials with tunable, programmable, and reconfigurable mechanical properties. Adv Funct Mater 2020:2004226.
[9] Zhang B, Li H, Cheng J, Ye H, Sakhaei AH, Yuan C, et al. Mechanically robust and UV-curable shape-memory polymers for digital light processing based 4D printing. Adv Mater 2021:2101298.
[10] Lin C, Zhang L, Liu Y, Liu L, Leng J. 4D printing of personalized shape memory polymer vascular stents with negative Poisson's ratio structure: a preliminary study. Sci China Technol Sci 2020;63(4):578–88.
[11] Lin C, Liu L, Liu Y, Leng J. Recent developments in next-generation occlusion devices. Acta Biomater 2021;128:100–19.
[12] Zhang B, Li HG, Cheng JX, Ye HT, Sakhaei AH, Yuan C, et al. Mechanically robust and UV-curable shape-memory polymers for digital light processing based 4D printing. Adv Mater 2021;33(27).
[13] Zhao Q, Li C, Shum HC, Du X. Shape-adaptable biodevices for wearable and implantable applications. Lab Chip 2020;20(23):4321–41.
[14] Zhao Q, Wang J, Cui H, Chen H, Wang Y, Du X. Programmed shape-morphing scaffolds enabling facile 3D endothelialization. Adv Funct Mater 2018:1801027.
[15] Lin C, Liu L, Liu Y, Leng J. 4D printing of shape memory polybutylene succinate/polylactic acid (PBS/PLA) and its potential applications. Compos Struct 2022;279:114729.
[16] Cui H, Miao S, Esworthy T, Lee S, Zhou X, Hann SY, et al. A novel near-infrared light responsive 4D printed nanoarchitecture with dynamically and remotely controllable transformation. Nano Res 2019;12(6SI):1381–8.
[17] Lin C, Liu L, Liu Y, Leng J. 4D printing of bioinspired absorbable left atrial appendage occluders: a proof-of-concept study. ACS Appl Mater Interfaces 2021;13(11):12668–78.
[18] Lin C, Lv J, Li Y, Zhang F, Li J, Liu Y, et al. 4D-Printed biodegradable and remotely controllable shape memory occlusion devices. Adv Funct Mater 2019:1906569. 0 (0).
[19] Morrison RJ, Hollister SJ, Niedner MF, Mahani MG, Park AH, Mehta DK, et al. Mitigation of tracheobronchomalacia with 3D-printed personalized medical devices in pediatric patients. Sci Transl Med 2015;7(285):264r–85r.
[20] Saidy NT, Wolf F, Bas O, Keijdener H, Hutmacher DW, Mela P, et al. Biologically inspired scaffolds for heart valve tissue engineering via melt electrowriting. Small 2019;15(24):1900873.
[21] Ma Q, Cheng H, Jang K, Luan H, Hwang K, Rogers JA, et al. A nonlinear mechanics model of bio-inspired hierarchical lattice materials consisting of horseshoe microstructures. J Mech Phys Solid 2016;90:179–202.
[22] Guo X, Ni X, Li J, Zhang H, Zhang F, Yu H, et al. Designing mechanical metamaterials with kirigami-inspired, hierarchical constructions for giant positive and negative thermal expansion. Adv Mater 2021;33(3):2004919.
[23] Yu H, Liang B, Zhao Z, Liu P, Lei H, Song W, et al. Metamaterials with a controllable thermal-mechanical stability: mechanical designs, theoretical predictions and experimental demonstrations. Compos Sci Technol 2021;207:108694.
[24] Ni X, Guo X, Li J, Huang Y, Zhang Y, Rogers JA. 2D mechanical metamaterials with widely tunable unusual modes of thermal expansion. Adv Mater 2019;31(48):1905405.
[25] Gao Z, Wang H, Letov N, Zhao YF, Zhang X, Wu Y, et al. Data-driven design of biometric composite metamaterials with extremely recoverable and ultrahigh specific energy absorption. Compos B Eng 2023;251:110468.
[26] Tao R, Ji L, Li Y, Wan Z, Hu W, Wu W, et al. 4D printed origami metamaterials with tunable compression twist behavior and stress-strain curves. Compos B Eng 2020;201:108344.
[27] Zhang L, Song B, Choi S, Yao Y, Shi Y. Anisotropy-inspired, simulation-guided design and 3D printing of microlattice metamaterials with tailored mechanical-transport performances. Compos B Eng 2022;236:109837.
[28] Chen B, Chen L, Du B, Liu H, Li W, Fang D. Novel multifunctional negative stiffness mechanical metamaterial structure: tailored functions of multi-stable and compressive mono-stable. Compos B Eng 2021;204:108501.
[29] Ma X, Duan Y, Huang L, Lei H, Yang X. Quasiperiodic metamaterials with broadband absorption: tailoring electromagnetic wave by Penrose tiling. Compos B Eng 2022;233:109659.
[30] Ma X, Duan Y, Huang L, Lei H, Yang X. Quasiperiodic metamaterials with broadband absorption: tailoring electromagnetic wave by Penrose tiling. Compos B Eng 2022;233:109659.
[31] Wang J, Zhao Q, Wang Y, Zeng Q, Wu T, Du X. Self-unfolding flexible microelectrode arrays based on shape memory polymers. Adv Mater Technol 2019;4(11):1900566.
[32] Zhao Q, Wang J, Wang Y, Cui H, Du X. A stage-specific cell-manipulation platform for inducing endothelialization on demand. Natl Sci Rev 2020;7(3):629–43.
[33] Liu J, Yan D, Pang W, Zhang Y. Design, fabrication and applications of soft network materials. Mater Today 2021;49:324–50.
[34] Yan D, Chang J, Zhang H, Liu J, Song H, Xue Z, et al. Soft three-dimensional network materials with rational bio-mimetic designs. Nat Commun 2020;11(1):1180.
[35] Wang D, Xiong Y, Zhang B, Zhang Y, Rosen D, Ge Q. Design framework for mechanically tunable soft biomaterial composites enhanced by modified horseshoe lattice structures. Soft Matter 2020;16(6):1473–84.
[36] Wang Z, Li N, Li R, Li Y, Ruan L. Biodegradable intestinal stents: a review. Prog Nat Sci: Mater Int 2014;24(5):423–32.
[37] Li G, Chen Y, Hu J, Wu X, Hu J, He X, et al. A 5-fluorouracil-loaded polydioxanone weft-knitted stent for the treatment of colorectal cancer. Biomaterials 2013;34(37):9451–61.
[38] Xie X, Zheng X, Han Z, Chen Y, Zheng Z, Zheng B, et al. A biodegradable stent with surface functionalization of combined-therapy drugs for colorectal cancer. Adv Healthc Mater 2018;7(24):e1801213.